


One-dimensional spin-polarized electron channel in the two-dimensional PbBi compound on siliconA. N. Mihalyuk^{1,2,*}, L. V. Bondarenko¹, A. Y. Tupchaya¹, T. V. Utas¹, Y. E. Vekovshinin^{1,2}, D. V. Gruznev¹, S. V. Ereemeev³, A. V. Zotov¹ and A. A. Saranin¹¹*Institute of Automation and Control Processes FEB RAS, 690041 Vladivostok, Russia*²*School of Natural Sciences, Far Eastern Federal University, 690950 Vladivostok, Russia*³*Institute of Strength Physics and Materials Science SB RAS, Tomsk 634055, Russia* (Received 13 May 2021; revised 21 July 2021; accepted 24 August 2021; published 7 September 2021)

Quantum phenomena at the ultimate atomic-scale two-dimensional limit attract increasing interest due to the emergence of exotic physics and potential applications in prospective electronic devices. In this work, we carried out a theoretical and experimental study of the atomic, electronic, and spin structures of the single-atomic-layer PbBi compounds grown on silicon surface. We found that adsorption of half-monolayer of Bi and half-monolayer of Pb onto Si(111) surface leads to the formation of an atomic layer consisting of rhombuslike motifs. The rhombuslike motifs are arranged into the $2\sqrt{3} \times 2\sqrt{3}$ and 2×2 periodical structures. In the $2\sqrt{3} \times 2\sqrt{3}$ -PbBi phase, the motifs are oriented according to the C_3 symmetry and this phase is characterized as a trivial insulating spin-split system. In the 2×2 -PbBi phase, the motifs are oriented along a single direction giving rise to a one-dimensional metallic spin-polarized electron channel, which is of great relevance for spintronic-based applications. We traced the origin of the one-dimensional electronic states in the two-dimensional PbBi compound and discussed the interplay of these one-dimensional states with the geometry of the phase.

DOI: [10.1103/PhysRevB.104.125413](https://doi.org/10.1103/PhysRevB.104.125413)**I. INTRODUCTION**

Low-dimensional materials with advanced electronic properties comprise an object of significant interest due to the wide range of prospective applications in the nanoelectronics and spintronics. Such systems provide a fruitful field for exploration of the interesting physical phenomena related, for example, to the various exotic spin-polarized electronic states, such as topological insulators and semimetals [1–3], hinge states in the coupled Rashba layers [4], charge density waves in the atomic chains [5], the Su-Schrieffer-Heeger topological states [6], the Shiba states realized in nanowires [7], and many others. However, despite the great fundamental interests, experimental realization of the one-dimensional (1D) systems in the real materials is quite difficult. For example, the growth of metal wires on semiconductor surfaces, such as Pb chains on Si(100) [8], Bi/In wires on Si(111) [9], Au nanoribbons on Ge(111) [10], requires ultra-high-vacuum environment and accurate control of various growth parameters.

Spin-orbit coupling (SOC) plays an important role in many electronic effects observed in quantum materials. In this regard, lead and bismuth, having the largest atomic SOC values, are believed to be very promising candidates for realizing exotic quantum properties. In particular, lead is known to form 1D atomic chains [8,11] providing prospects for the 1D spin-polarized electron transport. In the two-dimensional (2D) systems, lead is mostly known as plumbene [12,13] with a giant topologically nontrivial gap in the Dirac spectrum hosting gapless spin-momentum-locked topological edge states.

Recently, occurrence of the exotic hourglass surface states was predicted in a stacked hydrogenated plumbene [14]. The ultrathin Pb films on silicon and germanium surfaces were found to be superconductors [15] with indication on an increasing superconducting transition temperature with Bi alloying [16]. Moreover, the lead-based materials are also known as topological superconductors, such as Pb/Co/Si(111) compound with 1D dispersive in-gap edge states surrounding a 2D topological superconducting domain of lead [17]. In the ultrathin Bi films of a few bilayers, the 1D topological spin-polarized edge states were predicted [18–20] and observed [21,22], whereas the bulk Bi is known as a high-order topological insulator, possessing 1D hinge states [23]. A single-layer or bilayer phase of bismuth atoms, arranged into a honeycomb [24] or asymmetric washboard lattices [25], named as a bismuthene, yield the vivid example of a high-temperature quantum spin Hall material [26]. There are several Bi and Pb containing compounds in the bulk and on the surface, which were predicted and observed to be topological superconductors and topological semimetals [27,28]. In particular, it was predicted that the $Pb_3Bi/Ge(111)$ material hosts the topological superconductivity, arising from the interplay of the geometric phase and electron correlation [27,29]. However, the formation and properties of the Pb-Bi 2D alloys on the other semiconductor surfaces have not been so far investigated.

Motivated by the earlier observations that bismuth and lead have demonstrated a number of advanced properties in a variety of perspective materials, we merged them together on a silicon surface and investigated atomic, electronic, and spin structures of the grown compound. We discuss the interplay between the PbBi compound geometry and the peculiar electronic states emerging in the system. In the

*mih-alexey@yandex.ru

(Pb, Bi)/Si(111)- 2×2 phase, we predict the existence of the quasi-1D spin-polarized electron channel induced by a special atomic arrangement of the constituent elements.

II. EXPERIMENTAL AND COMPUTATIONAL DETAILS

Experiments were performed in the ultrahigh-vacuum Omicron MULTIPROBE system (base pressure $\leq 2.0 \times 10^{-10}$ Torr) by means of scanning tunneling microscopy (STM) and low-energy electron diffraction (LEED) methods. Atomically clean Si(111) 7×7 surfaces were prepared *in situ* by flashing to 1280 °C after the samples were first outgassed at 600 °C for several hours. Pb and Bi were deposited from heated tantalum tubes and deposition rates was calibrated using STM observation of corresponding Pb and Bi reconstructions of Si(111) surface. During the Pb deposition onto the Si surface the sample temperature was held in the range from 100 °C to 200 °C by indirect heating. In this temperature range, the temperature was measured by a *K*-type thermocouple installed into the sample stage. STM images were acquired using Omicron variable-temperature STM-XA operating in a constant-current mode. Mechanically cut PtIr tips were used as STM probes after annealing in vacuum.

Density functional theory (DFT) calculations were performed using Vienna *ab initio* simulation package (VASP) [30,31], with core electrons represented by projector augmented wave (PAW) potentials [32]. The generalized gradient approximation of Perdew, Burke, and Ernzerhof (GGA-PBE) [33] to the exchange-correlation functional was employed for structure relaxation. To simulate the PbBi structure on Si(111) surface we used a slab consisting of 5 bilayers (BL) of the substrate with the PBE-optimized bulk Si lattice constant. Hydrogen atoms were used to passivate the Si dangling bonds at the bottom of the slab. The atomic positions of PbBi atoms and atoms of Si layers within the two topmost BLs of the slab were optimized. The geometry optimization was performed until the residual forces on atoms became smaller than 10 meV/Å. The $7 \times 7 \times 1$ and $5 \times 5 \times 1$ *k*-point mesh was used to sample the (Pb,Bi)/Si(111)- 2×2 and (Pb,Bi)/Si(111) $2\sqrt{3} \times 2\sqrt{3}$ surface Brillouin zones, respectively. For getting an accurate Si band gap we applied the DFT- $\frac{1}{2}$ self-energy correction method [34,35]. The scalar relativistic effects and the spin-orbit coupling (SOC) were taken into account for calculating the band structure of Si-based system. In order to find the most stable PbBi structures on Si(111) surface we used the *ab initio* random structure searching (AIRSS) approach [36].

III. RESULTS AND DISCUSSION

A. Samples preparation

STM and LEED experiments have revealed that adsorption of about 0.5 ML (monolayer, 7.8×10^{14} cm $^{-2}$) of Bi and about 0.5 ML of Pb onto the Si(111) surface results in simultaneous formation of the two new reconstructions at the surface, the (Pb, Bi)/Si(111)- 2×2 (hereinafter referred to as 2×2) and the (Pb, Bi)/Si(111)- $2\sqrt{3} \times 2\sqrt{3}$ (hereinafter referred to as $2\sqrt{3} \times 2\sqrt{3}$). These reconstructions form in the (150–350) °C temperature range and can be built either by room-temperature (RT) deposition of both adsorbates followed by annealing or using successive depositions

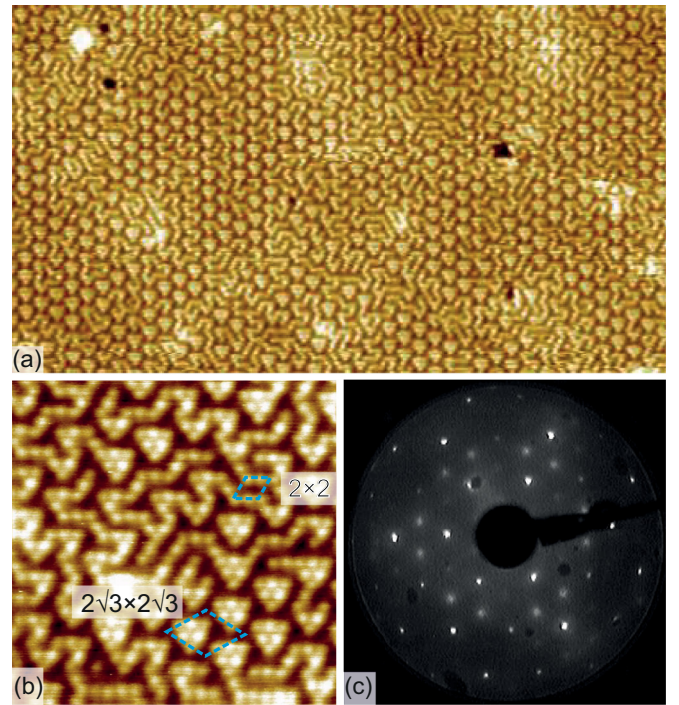


FIG. 1. 2×2 and $2\sqrt{3} \times 2\sqrt{3}$ reconstructions in (Pb, Bi)/Si(111) system with equilibrium Bi : Pb coverage ratio (0.5 ML of Bi and 0.5 ML of Pb). (a) 50×28 nm 2 (−1.5 V, 0.6 nA) STM image; (b) 10×10 nm 2 (−1.5 V, 0.1 nA) STM image; (c) 54 eV LEED pattern, recorded at 78 K.

with intermediate annealing after the first adsorbate (Pb or Bi) has been deposited. Usually, these procedures result in the formation of the surface containing a mixture of small domains (1–3 nm in size) of both 2×2 and $2\sqrt{3} \times 2\sqrt{3}$ phases. Typical large-scale STM image of such surface is shown in Fig. 1(a). One can see that surface is composed of the triangular shapes and meandering one-dimensional chains. Closer look [see the high-resolution STM image in Fig. 1(b)] reveals that the triangular shapes form the $2\sqrt{3} \times 2\sqrt{3}$ periodicity and the meandering chains the 2×2 periodicity with fluent transitions between them.

LEED observations [Fig. 1(c)] confirm the simultaneous presence of both reconstructions. One can notice that the 2×2 spots are quite sharp, while the $2\sqrt{3} \times 2\sqrt{3}$ spots are blurred because of a small size of the domains. From simple geometric considerations, one can conclude that the $2\sqrt{3} \times 2\sqrt{3}$ periodicity cannot create an anti-phase boundary inside the 2×2 domain, but vice versa the 2×2 periodicity can create an antiphase boundary inside the $2\sqrt{3} \times 2\sqrt{3}$ domain. Small size of the domains results in a frequent $2a_{\text{Si}}$ [a_{Si} is the Si(111)- 1×1 surface lattice constant, 3.84 Å] phase shifts for the $2\sqrt{3} \times 2\sqrt{3}$ periodicity, whereas the 2×2 periodicity always remains in phase. Hence, the $2\sqrt{3} \times 2\sqrt{3}$ LEED spots are blurred and the 2×2 spots are sharp.

Sizes of the reconstruction domains and relative fractions of surface occupied by each of the reconstructions, 2×2 or $2\sqrt{3} \times 2\sqrt{3}$, were always about the same, irrespective of the annealing temperature. Typically, the 2×2 and $2\sqrt{3} \times 2\sqrt{3}$ areas relate to each other approximately as three to one.

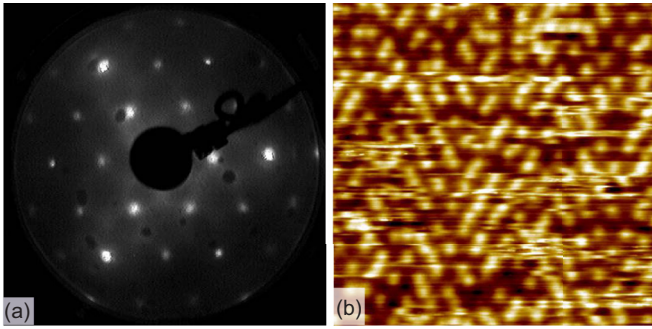


FIG. 2. Defective 2×2 reconstruction in (Pb,Bi)/Si(111) system obtained by increasing partial Bi coverage (surface with 0.33 Pb and 0.67 ML Bi). (a) 54 eV LEED pattern, recorded at 78 K; (b) $10 \times 10 \text{ nm}^2$ (-1.5 V , 0.5 nA) STM image recorded at room temperature.

Areal fraction of the 2×2 can be increased by increasing Bi coverage keeping the total metal coverage close to 1 ML. The resultant surface can be completely covered by the 2×2 reconstruction. The undesirable side effect of this procedure is a noticeable loss in the reconstruction ordering. The LEED pattern from such surface [Fig. 2(a)] displays diffusive 2×2 spots. In the STM image from the surface [Fig. 2(b)], one can see that the 2×2 chains are fractured or even appear as separate protrusions.

Figures 3(a) and 3(b) present the high-resolution STM images of the same place on a mixed PbBi/Si(111) surface (2×2 and $2\sqrt{3} \times 2\sqrt{3}$) recorded in the filled and empty states, respectively. One can clearly see that STM appearance of the surface at the opposite bias polarities is quite different. In the filled-state STM image, the pattern is formed by more or less separate protrusions which are lined up either in the 2×2 chains or in the $2\sqrt{3} \times 2\sqrt{3}$ triangles. Empty-state STM image demonstrates essentially a honeycomb appearance with approximately 2×2 periodicity and some distortions related to the different domains of the 2×2 and $2\sqrt{3} \times 2\sqrt{3}$ elements.

B. Atomic structure

In order to find the ground-state structural models for both 2×2 and $2\sqrt{3} \times 2\sqrt{3}$ phases, we performed comprehen-

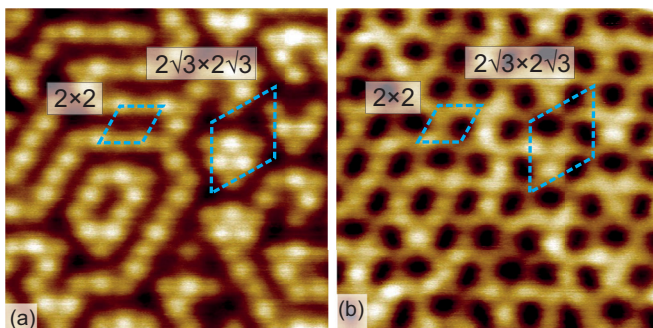


FIG. 3. High-resolution STM images of 2×2 and $2\sqrt{3} \times 2\sqrt{3}$ reconstructions in (Pb,Bi)/Si(111) system recorded at the same place of the surface in (a) filled (-1.0 V) and (b) empty ($+1.0 \text{ V}$) states.

sive DFT total-energy calculations applying *ab initio* random structure searching (AIRSS) method for models with both Pb and Bi coverages to be 0.5 ML as follows from the experiment. Figures 4(a) and 4(b) illustrate an atomic arrangement of the found ground-state models shown in the top and side views. The 2×2 structural model appears to be more stable than the $2\sqrt{3} \times 2\sqrt{3}$ one, by 5 meV per 1×1 Si surface cell. Such a small energy difference between two phases explains the simultaneous appearance of these reconstructions in the STM with a minor preference for the 2×2 phase. Remarkably, their arrangement is based on the same rhombuslike motif [hatched in yellow in Figs. 4(a) and 4(b)]. This motif is composed of two Bi and two Pb atoms located almost in the on-top (T1) sites on the bulk-truncated Si(111) surface. Within the motif, Bi dimer forms a short rhombus diagonal (yielding 3.1 \AA), while the two separated Pb atoms bonded to Bi atoms form a long rhombus diagonal (yielding 5.8 \AA). The 2×2 phase is composed of rhombi with a single orientation [outlined in Fig. 4(a) by red oval]. The unit cell of the $2\sqrt{3} \times 2\sqrt{3}$ phase contains three rhombi rotated from each other by 60° [as shown in Fig. 4(b) by red, blue, and green ovals], thus, arranged in the sixfold starlike structure.

Figures 4(c) and 4(d) present a comparison of the DFT simulated and experimental STM images for the 2×2 and $2\sqrt{3} \times 2\sqrt{3}$ reconstructions, respectively. As one can see, the coincidence is fairly good supporting validity of the AIRSS-derived structural models. Detailed consideration of STM images reveals that at the negative bias (or filled states) the main pattern is formed by bright protrusions associated with Pb atoms, while at the positive bias (or empty states) the main pattern has bright networklike form associated with silicon atoms.

C. Electronic properties

Before starting the examination of the electronic band structure of the two systems, it is worth noting that in spite of the C_{3v} symmetry of the underlying Si(111) substrate, the PbBi compound in the 2×2 phase has a C_{1h} symmetry arising from a particular arrangement of the constituent rhombus motifs, while in the $2\sqrt{3} \times 2\sqrt{3}$ phase the C_{3v} total symmetry is preserved.

The results of the electronic band-structure calculations for the (Pb,Bi)/Si(111)- 2×2 system are summarized in Fig. 5. In the nonrelativistic spectrum [Figs. 5(a) and 5(b)], the two highly dispersing S1 and S2 bands propagate within the silicon bulk gap. According to Figs. 5(a) and 5(b), the S1 band is formed mainly by Bi p_y states, while the S2 band is formed by Pb p_x states. The hybridization of S1 and S2 bands results in appearance of 70-meV gap just below the Fermi level in the middle of the $\bar{M}-\bar{K}$ direction.

Including the SOC in the band-structure calculations leads to a lift up of the spin degeneracy [Fig. 5(c)] that in turn results a closure of the hybridization gap and gives rise to electron and holelike spin-split bands at the \bar{M} point. Notice that the spin splitting in the $\bar{M}-\bar{\Gamma}$ direction is insignificant, while along the $\bar{M}-\bar{K}$ the spin splitting is huge for the electron band, and it is even much larger for the holelike band. However, the symmetry of the 2×2 hexagonal surface Brillouin zone (SBZ) does not reflect the C_{1h} symmetry of the PbBi compound.

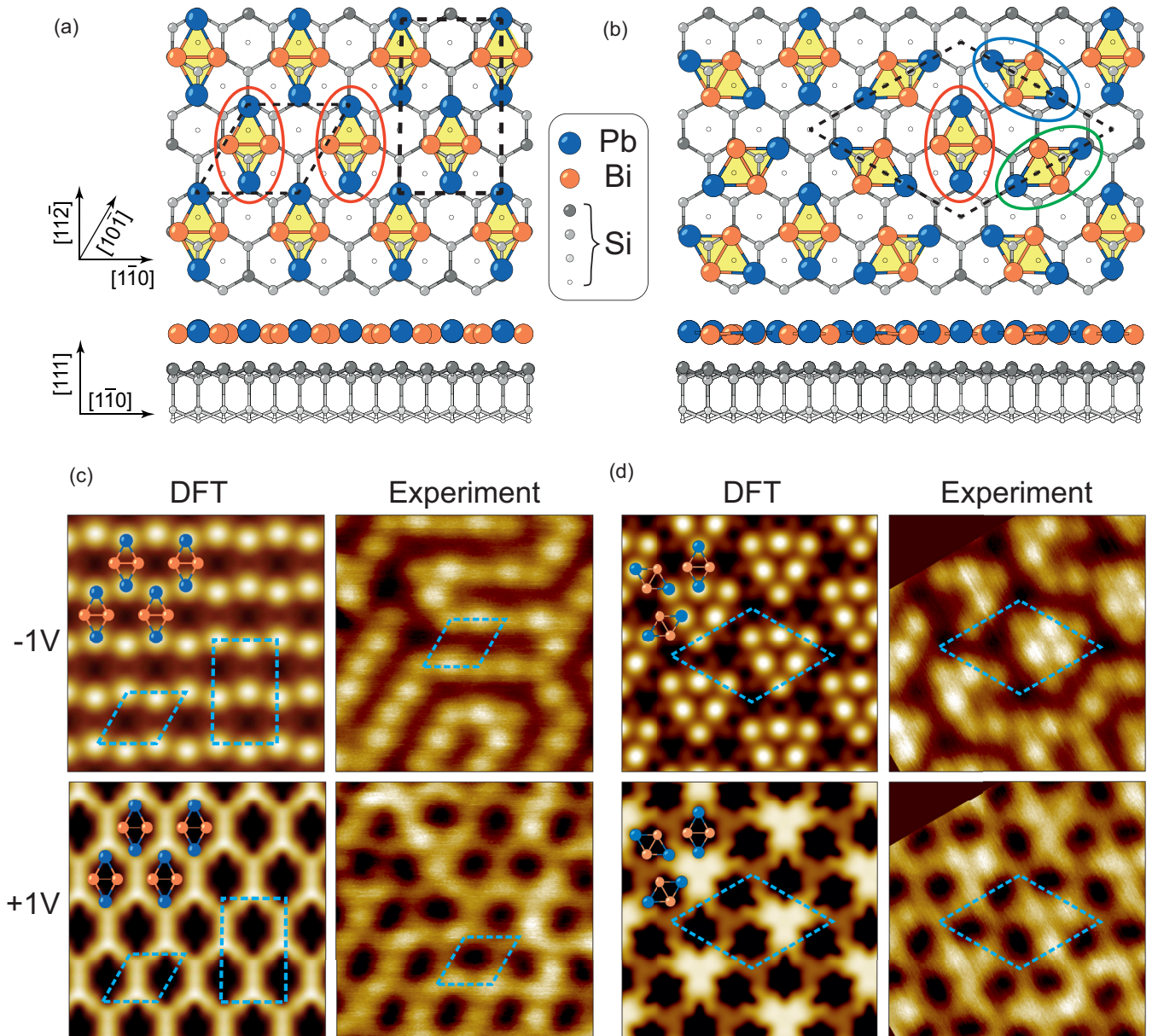


FIG. 4. Atomic models (a), (b) and comparison of DFT simulated and experimental STM images (c), (d) for 2×2 and $2\sqrt{3} \times 2\sqrt{3}$ reconstructions in (Pb,Bi)/Si(111) system. In (a) and (b) four-atomic PbBi rhombus patterns are highlighted by yellow color to simplify comparison with STM images. In (c) and (d) top rows represent comparison of DFT simulated and experimental STM images for filled states (-1 V) and bottom rows the same for empty states ($+1$ V).

The calculated electronic spectrum of the $2 \times 2\sqrt{3}$ rectangular cell, which represents the unidimensional arrangement of PbBi rhombi in the 2×2 phase, is shown in Fig. 5(d). Due to the Brillouin zone folding [see inset in Fig. 5(d)] the spin-split bands, presented along the \bar{M} - \bar{K} direction of 2×2 hexagonal SBZ, appear in the $\bar{\Gamma}$ - \bar{X} direction of the rectangular SBZ.

It is worth noting that in-plane spin component has a significant value only for the Bi-derived states, while the Pb-derived states have negligible values [Fig. 5(d)], but the out-of-plane spin component is significant for both electron and holelike bands in the vicinity of the $\bar{\Gamma}$ point, and decreases towards the \bar{X} (\bar{X}') points of the rectangular SBZ [Fig. 5(f)]. Figure 5(g) shows the volumetric view of the surface bands and highlights their complicated spin texture.

Figure 5(e) shows the constant energy contours at different energies. In particular, it is seen that the unoccupied part of the spectrum (above the degeneracy point of the electron spin-split band) is characterized by the highly anisotropic constant energy contours elongated along the \bar{X} - $\bar{\Gamma}$ - \bar{X} direction and which are almost degenerate along the $\bar{\Gamma}$ - \bar{Y} direction. At the Fermi level, there is a pair of anisotropic spin-polarized hole pockets in the middle of the $\bar{\Gamma}$ - \bar{X} directions. Meanwhile, the highly anisotropic shape of the hole pockets and character of their spin polarization are retained until -75 meV (top of the silicon valence band). So, within the $[-75; 0]$ meV energy range a quasi-1D electron channel persists in the spectrum [hatched in yellow stripe in Figs. 5(c) and 5(f)], wherein the spin orientations of the two hole pockets have opposite

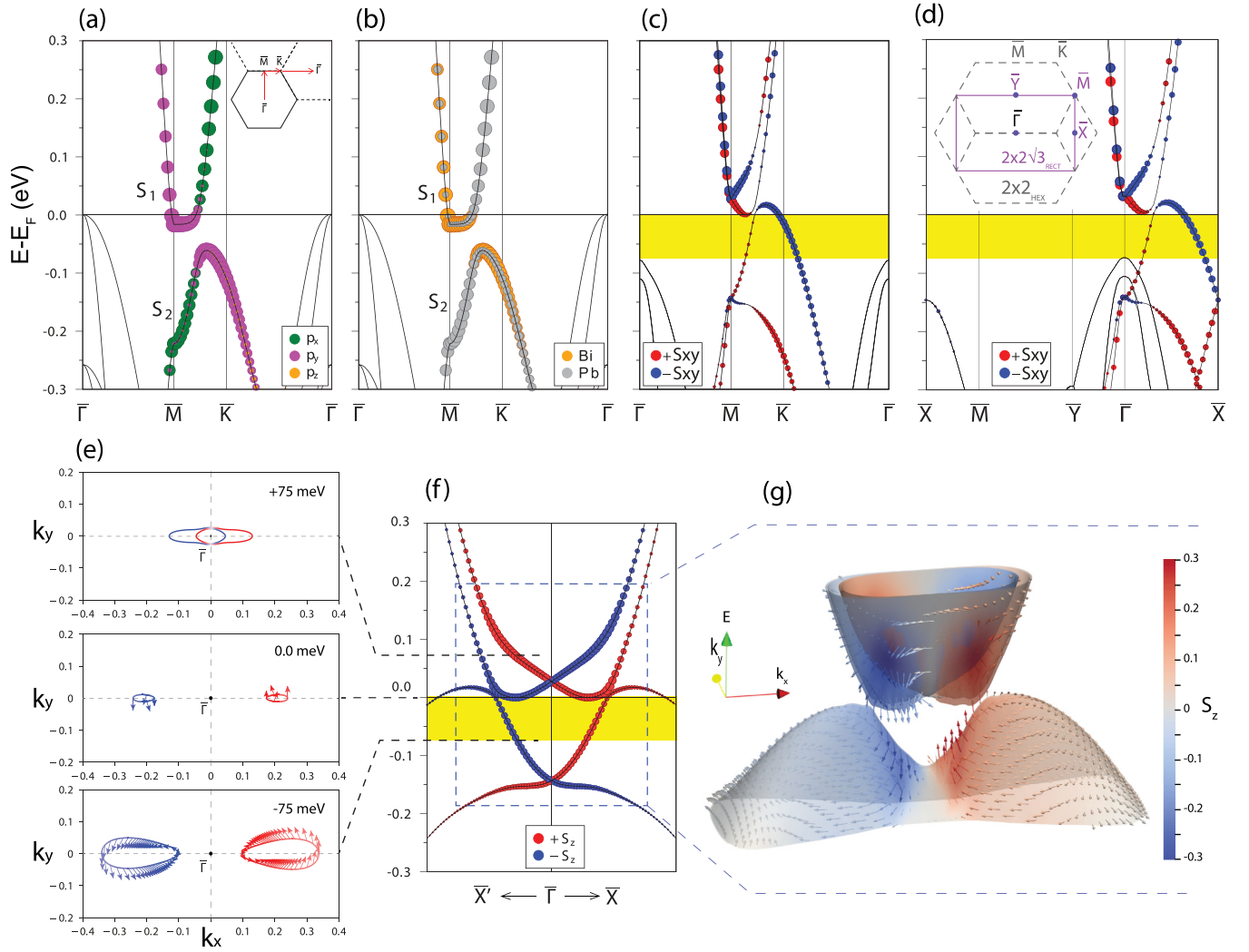


FIG. 5. Electronic properties of 2×2 -PbBi phase. (a), (b) Orbital- and elements-projected nonrelativistic spectra, respectively, calculated along high-symmetry directions of the 2×2 SBZ shown in the inset at (a). (c) Spin-polarized relativistic spectrum with in-plane spin component, where quasi-1D electron channel is marked by yellow stripe. (d) Spin-polarized relativistic spectrum calculated along high-symmetry directions of the $2 \times 2\sqrt{3}$ rectangular surface BZ (see inset). (e) Evolution of the Fermi-surface geometry with respect to different energies (the size of arrows defines the size of in-plane component, and the color defines the sign of out-of-plane spin component). (f) Electronic spectrum along $\bar{X}'-\bar{\Gamma}-\bar{X}$ with out-of-plane spin projection, where the symbol size corresponds to the magnitude of the respective S_z components. (g) Volumetric visualization of 2×2 -PbBi bands and associated spin texture.

directions, and hence the electron backscattering is forbidden. The nonrelativistic spectrum of the (Pb,Bi)/Si(111)- $2\sqrt{3} \times 2\sqrt{3}$ phase [Fig. 6(a)] has an insulating character with electronic dispersion characterized by a gap between a bunch of the weakly dispersive PbBi bands propagating at 0.6 eV above E_F and the top of the silicon bulk valence band (VB). The unoccupied bands of the PbBi layer are formed by the mixture of Bi and Pb $p_{x,y}$ orbitals, while the occupied states, lying within Si VB, are characterized by the mixture of $p_{x,y}$ and p_z orbitals.

The insulating character of the band structure is retained in the presence of SOC effect [Fig. 6(b)], which leads to the band splitting over the entire k space of spectrum. Importantly that in contrast to the 2×2 -PbBi phase the dispersions now have a clear isotropic character with the spin components following the behavior typical for the Rashba helicity. For instance, the occupied Rashba-split band at the \bar{M} point displays a common

2D character. The insulating character of the $2\sqrt{3} \times 2\sqrt{3}$ -PbBi phase may be traced from the structural considerations. In particular, in its atomic model all Pb atoms (accumulating the charges) are arranged in the form of isolated triangular clusters [as shown in Fig. 4(d)] and are separated from each other by the nonmetallic bismuth atoms; consequently, such an atomic configuration gives rise to the insulating character of the system. It is in contrast to the 2×2 -PbBi phase where motifs are arranged in the single direction that leads to the formation of the Pb charge chains [Fig. 4(c)] providing an existence of the 1D metallic states.

IV. CONCLUSIONS

In conclusion, we carried out an experimental and theoretical study of structural and electronic properties of PbBi single atomic layer arranged on Si(111) surface. There are two

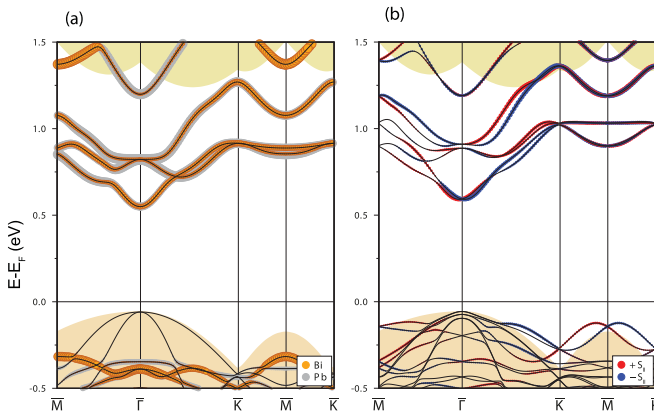


FIG. 6. Electronic properties of $2\sqrt{3} \times 2\sqrt{3}$ -PbBi phase. (a) Elements-projected nonrelativistic spectrum. The elemental characters of the bands are shown by orange and gray colors for Bi and Pb atoms, respectively, (b) spin-polarized relativistic spectrum with in-plane spin component, where red and blue balls correspond to respective in-plane spin components. In both figures symbols are very close to each other resulting in bands instead of individual balls.

coexisting phases with 2×2 and $2\sqrt{3} \times 2\sqrt{3}$ periodicities, as revealed by STM and LEED observations. We established the ground-state atomic models by *ab initio* random structure searching method for both phases, which geometries are determined by the orientation and number of constituent PbBi rhombuslike motifs. Simulated STM images of the found structural models are in a good agreement with the STM observations.

Electronic band-structure calculations revealed the intricate details of the interplay between the atomic structure and electronic properties of two PbBi phases. The arrangement of the rhombuslike motifs, either with C_{1h} or C_{3v} symmetry, determines the anisotropy of the electronic states and the metallic/insulator character of the system. The (Pb, Bi)/Si(111)- 2×2 phase is characterized by the sizable anisotropy of the band structure demonstrating a spin-polarized quasi-1D electron channel within 75 meV energy range in the vicinity of the Fermi level. The second coexisting (Pb, Bi)/Si(111)- $2\sqrt{3} \times 2\sqrt{3}$ phase has an insulating character with a large gap, and its electronic states are not overlapping with the 1D electron channel of the (Pb, Bi)/Si(111)- 2×2 phase. So, the electronic structure of the sample even with the two coexisting phases still will be characterized by the 1D spin-polarized electronic states. The present findings on the peculiar electronic properties produced by PbBi compound formation on the semiconductor surfaces might open opportunities for creating new advanced electronic phases and a realization of anisotropic charge and spin transport.

ACKNOWLEDGMENTS

The work was supported by the RSF Grant No. 19-12-00101. The calculations were partly supported by the Government research assignment for ISPMs SB RAS, Project No. FWRW-2019-0032. The calculations were conducted using the equipment of Shared Resource Center Far Eastern Computing Resource IACP FEB RAS [37].

- [1] P. Liu, J. R. Williams, and J. J. Cha, Topological nanomaterials, *Nat. Rev. Mater.* **4**, 479 (2019).
- [2] M. Z. Hasan and C. L. Kane, Colloquium: Topological insulators, *Rev. Mod. Phys.* **82**, 3045 (2010).
- [3] H. Weng, X. Dai, and Z. Fang, Topological semimetals predicted from first-principles calculations, *J. Phys.: Condens. Matter* **28**, 303001 (2016).
- [4] K. Plekhanov, F. Ronetti, D. Loss, and J. Klinovaja, Hinge states in a system of coupled Rashba layers, *Phys. Rev. Research* **2**, 013083 (2020).
- [5] H. W. Yeom, S. Takeda, E. Rotenberg, I. Matsuda, K. Horikoshi, J. Schaefer, C. M. Lee, S. D. Kevan, T. Ohta, T. Nagao, and S. Hasegawa, Instability and Charge Density Wave of Metallic Quantum Chains on a Silicon Surface, *Phys. Rev. Lett.* **82**, 4898 (1999).
- [6] D. Obana, F. Liu, and K. Wakabayashi, Topological edge states in the Su-Schrieffer-Heeger model, *Phys. Rev. B* **100**, 075437 (2019).
- [7] F. Pientka, L. I. Glazman, and F. von Oppen, Topological superconducting phase in helical Shiba chains, *Phys. Rev. B* **88**, 155420 (2013).
- [8] A. N. Mihalyyuk, J. P. Chou, S. V. Ereemeev, A. V. Zotov, and A. A. Saranin, One-dimensional Rashba states in Pb atomic chains on a semiconductor surface, *Phys. Rev. B* **102**, 035442 (2020).
- [9] T. Tanaka and Y. Gohda, First-principles prediction of one-dimensional giant Rashba splittings in Bi-adsorbed In atomic chains, *Phys. Rev. B* **98**, 241409(R) (2018).
- [10] E. H. Do, S. G. Kwon, M. H. Kang, and H. W. Yeom, Structural and electronic effects of adatoms on metallic atomic chains in Si(111) 5×2 -Au, *Sci. Rep.* **8**, 15537 (2018).
- [11] M. Kociuszyński, A. Stepniak-Dybala, M. Dachniewicz, L. Żurawek, M. Krawiec, and R. Zdyb, Hut-shaped lead nanowires with one-dimensional electronic properties, *Phys. Rev. B* **102**, 125415 (2020).
- [12] H. Zhao, C.-W. Zhang, W.-X. Ji, R.-W. Zhang, S.-S. Li, S.-S. Yan, B.-M. Zhang, P. Li, and P.-J. Wang, Unexpected giant-gap quantum spin Hall insulator in chemically decorated plumbene monolayer, *Sci. Rep.* **6**, 20152 (2016).
- [13] J. Yuhara, B. He, N. Matsunami, M. Nakatake, and G. Le Lay, Graphene's latest cousin: Plumbene epitaxial growth on a "nano watercube", *Adv. Mater.* **31**, 1901017 (2019).
- [14] G. Gao, H. Huan, H. Bao, Y. Xue, B. Zhao, R. Yu, and Z. Yang, Prediction of Dirac semimetals and hourglass surface states in stacked hydrogenated Xenes ($X = \text{Sn}$ and Pb), *Phys. Rev. B* **102**, 205114 (2020).
- [15] T. Zhang, P. Cheng, W.-J. Li, Y.-J. Sun, G. Wang, X.-G. Zhu, K. He, L. Wang, X. Ma, X. Chen, Y. Wang, Y. Liu, H.-Q. Lin, J.-F. Jia, and Q.-K. Xue, Superconductivity in one-atomic-layer metal films grown on Si(111), *Nat. Phys.* **6**, 104 (2010).

- [16] M. M. Özer, Y. Jia, Z. Zhang, J. R. Thompson, and H. H. Weiering, Tuning the quantum stability and superconductivity of ultrathin metal alloys, *Science* **316**, 1594 (2007).
- [17] G. C. Menard, S. Guissart, C. Brun, R. T. Leriche, M. Trif, F. F. Debontridder, D. Demaille, D. Roditchev, P. Simon, and T. Cren, Two-dimensional topological superconductivity in Pb/Co/Si(111), *Nat. Commun.* **8**, 2040 (2017).
- [18] S. Murakami, Quantum Spin Hall Effect and Enhanced Magnetic Response by Spin-Orbit Coupling, *Phys. Rev. Lett.* **97**, 236805 (2006).
- [19] Z. Liu, C.-X. Liu, Y.-S. Wu, W.-H. Duan, F. Liu, and J. Wu, Stable Nontrivial Z_2 Topology in Ultrathin Bi (111) Films: A First-Principles Study, *Phys. Rev. Lett.* **107**, 136805 (2011).
- [20] Z. F. Wang, L. Chen, and F. Liu, Tuning topological edge states of Bi(111) bilayer film by edge adsorption, *Nano Lett.* **14**, 2879 (2014).
- [21] Y. Lu, W. Xu, M. Zeng, G. Yao, L. Shen, M. Yang, Z. Luo, F. Pan, K. Wu, T. Das, P. He, J. Jiang, J. Martin, Y. P. Feng, H. Lin, and X.-s. Wang, Topological properties determined by atomic buckling in self-assembled ultrathin Bi(110), *Nano Lett.* **15**, 80 (2015).
- [22] I. K. Drozdov, A. Alexandradinata, S. Jeon, S. Nadj-Perge, H. Ji, R. J. Cava, B. Andrei Bernevig, and A. Yazdani, One-dimensional topological edge states of bismuth bilayers, *Nat. Phys.* **10**, 664 (2014).
- [23] F. Schindler, Z. Wang, M. G. Vergniory, A. M. Cook, A. Murani, S. Sengupta, A. Y. Kasumov, R. Deblock, S. Jeon, I. Drozdov, H. Bouchiat, S. Guéron, A. Yazdani, B. A. Bernevig, and T. Neupert, Higher-order topology in bismuth, *Nat. Phys.* **14**, 918 (2018).
- [24] F. Reis, G. Li, L. Dudy, M. Bauernfeind, S. Glass, W. Hanke, R. Thomale, J. Schäfer, and R. Claessen, Bismuthene on a SiC substrate: A candidate for a high-temperature quantum spin Hall material, *Science* **357**, 287 (2017).
- [25] E. Aktürk, O. U. Aktürk, and S. Ciraci, Single and bilayer bismuthene: Stability at high temperature and mechanical and electronic properties, *Phys. Rev. B* **94**, 014115 (2016).
- [26] W. Luo and H. Xiang, Room temperature quantum spin Hall insulators with a buckled square lattice, *Nano Lett.* **15**, 3230 (2015).
- [27] L. Li, S. Ren, W. Qin, S. Zhang, X. Wan, Y. Jia, P. Cui, and Z. Zhang, Emergence of Van Hove singularity and topological states in $Pb_3Bi/Ge(111)$ Rashba systems, *Phys. Rev. B* **102**, 035150 (2020).
- [28] I. Di Bernardo, J. Hellerstedt, C. Liu, G. Akhgar, W. Wu, S. A. Yang, D. Culcer, S.-K. Mo, S. Adam, M. T. Edmonds, and M. S. Fuhrer, Progress in epitaxial thin-film Na_3Bi as a topological electronic material, *Adv. Mater.* **33**, 2005897 (2021).
- [29] W. Qin, L. Li, and Z. Zhang, Chiral topological superconductivity arising from the interplay of geometric phase and electron correlation, *Nat. Phys.* **15**, 796 (2019).
- [30] G. Kresse and J. Hafner, *Ab initio* molecular dynamics for liquid metals, *Phys. Rev. B* **47**, 558 (1993).
- [31] G. Kresse and J. Furthmüller, Efficient iterative schemes for *ab initio* total-energy calculations using a plane-wave basis set, *Phys. Rev. B* **54**, 11169 (1996).
- [32] P. E. Blöchl, Projector augmented-wave method, *Phys. Rev. B* **50**, 17953 (1994).
- [33] J. P. Perdew, K. Burke, and M. Ernzerhof, Generalized Gradient Approximation Made Simple, *Phys. Rev. Lett.* **77**, 3865 (1996).
- [34] L. G. Ferreira, M. Marques, and L. K. Teles, Approximation to density functional theory for the calculation of band gaps of semiconductors, *Phys. Rev. B* **78**, 125116 (2008).
- [35] L. G. Ferreira, M. Marques, and L. K. Teles, Slater half-occupation technique revisited: The LDA-1/2 and GGA-1/2 approaches for atomic ionization energies and band gaps in semiconductors, *AIP Adv.* **1**, 032119 (2011).
- [36] C. J. Pickard and R. J. Needs, *Ab initio* random structure searching, *J. Phys.: Condens. Matter* **23**, 053201 (2011).
- [37] <https://cc.dvo.ru>.